Microbubbles

DOI: 10.1002/anie.201007377

Tunable Synthesis of Encapsulated Microbubbles by Coupled Electrophoretic Stabilization and Electrochemical Inflation**

*Yu-Wen Huang, Faisal A. Shaikh, and Victor M. Ugaz**

Microbubbles are immensely important targeted therapeutic delivery vehicles and imaging contrast agents. But they are also incredibly challenging to manufacture and store owing to extreme internal pressures generated by the high surface curvature at these small size scales. Here we show how these limitations can be overcome by exploiting an interplay between microscale electrokinetics and electrochemistry that simultaneously confines macromolecular encapsulants near an electrode surface while inflating them with gases evolved from electrochemical reactions localized there. Stabilized microbubbles incorporating a remarkably broad range of morphologies can be produced by manipulating these fundamental processes. We demonstrate this versatility by generating dense clouds of small microbubbles that enable label-free detection of virtually any charged macromolecule, and by synthesizing larger discrete encapsulated microbubbles of tunable size.

The inherent instability of microbubbles—that is, gas-filled bubbles in the 1–50 μm size range—results from the enormous Laplace pressures imposed by their highly curved interfacial topologies.[1] Macromolecular encapsulants (e.g., amphiphilic surfactants, lipids) are often employed as stabilization agents to counter these extreme conditions by bolstering the interfacial barrier against gas outflow.[2] The resulting stabilized microbubbles offer unique properties that have long been appreciated in the context of affinity separations (i.e., colloidal gas apherons),[3] and more recently as contrast agents for ultrasound imaging,[4] as well as convenient platforms for tethering chemical compounds (receptors, antibodies, etc.) to enable highly specific in vivo targeting (either to precisely deliver drug payloads or to locally destroy surrounding tissue when ruptured by an applied ultrasonic field).[2b,5] But despite these exciting applications, conventional batch-scale approaches used to produce encapsulated microbubbles are often relatively crude, based on mechanical agitation to entrain surrounding gas. Incredible progress has been made toward development of improved strategies at both the macro-scale (e.g., sonication and emulsification)[6] and micro-scale (e.g., flow focusing and T-junctions),[7] but a critical need still exists for approaches offering greater robustness to tune microbubble sizes and properties, as well as providing scalability from large batches to single-dose amounts.

We have developed an electrokinetically actuated microbubble synthesis method that addresses these needs by establishing localized zones inside a microchannel network where an encapsulant can become enriched to a very high concentration while simultaneously experiencing infusion with electrochemically generated gases. The cornerstone of our approach is a microfluidic system incorporating arrays of individually addressable electrodes (patterned along the microchannel floor) that make it possible to transport charged macromolecules from the bulk solution to an electrode surface where they become compacted into an ultra-thin film (Figure 1a).[8] This design enables very small potentials (1–3 V) to produce high electric fields (hundreds of $V\,cm^{-1}$) because of the close inter-electrode spacings (tens to hundreds of μm) achievable within the array. The compaction process is illustrated by observing the behavior of fluorescently labeled DNA in response to a 1 V DC potential applied across neighboring electrodes. The negatively charged DNA contained between active electrodes migrates toward the anode and experiences local enrichment, yielding a fluorescent zone at the electrode surface (Figure 1b). Remarkably, we discovered that this compacted film can also be clearly seen under ordinary white light even when the DNA sample is unlabeled, with no excitation or emission filters in the optical path (Figure 1c). An anomalous highly reflective zone is formed at the electrode surface that is most clearly evident under oblique illumination, becoming visible within 10–20 s and completely dissipating within 5–10 s after the voltage is switched off (Figure 1d–g). This unexpected phenomenon can be widely applied, making it possible to detect a variety of unlabeled macromolecules including proteins (Figure 1h–j) and small-molecule cyclodextrans (Figure 1k). The effect can be tuned to localize compaction at either the anode or cathode by adjusting the buffer pH relative to the sample's isoelectric point (Figure 1i).

To determine the morphology of the compacted macromolecular films, we repeated the above mentioned DNA capture experiments under transmitted illumination using optically transparent thin gold electrode arrays. Observing the process under polarized light reveals that dense stabilized microbubble clouds are embedded within the enriched DNA

[*] Y.-W. Huang, F. A. Shaikh, Prof. V. M. Ugaz
Artie McFerrin Department of Chemical Engineering
Texas A&M University, 3122 TAMU
College Station, TX 77843 (USA)
Fax: (+1) 979-458-1002
E-mail: ugaz@tamu.edu

[**] This work was supported in part by the Camille & Henry Dreyfus Foundation and the US National Science Foundation (NSF) under grant CTS-0554108. We thank Prof. Gyula Vigh for graciously providing cyclodextran samples, as well as for many helpful discussions. We also thank the staff in the Materials Characterization Facility (MCF) and the Microscopy & Imaging Center (MIC) at Texas A&M. V.M.U. gratefully acknowledges support from the K. R. Hall Professorship at Texas A&M.

Supporting information for this article is available on the WWW under http://dx.doi.org/10.1002/anie.201007377.

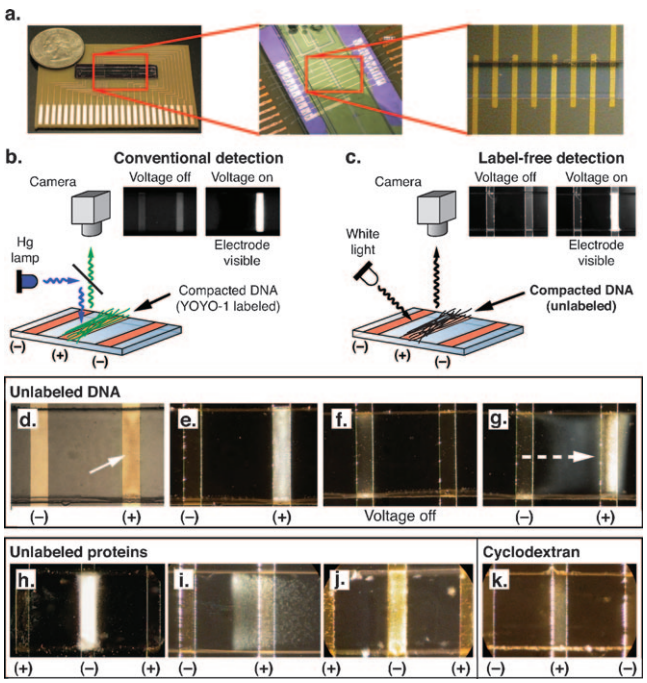

Figure 1. a) Microdevice design incorporating a glass microchannel (275×45 μm cross-section) bonded to a Si substrate patterned with an Pt microelectrode array (50 μm wide, 250 μm edge-to-edge spacing). b) Compaction of DNA fluorescently labeled with YOYO-1 dye yields a bright zone at the anode upon application of 1–2 V. c) At higher potentials (2.5 V), the same arrangement enables detection of unlabeled DNA under oblique white light illumination. d–g) Label-free detection of a 100 bp dsDNA ladder sample initially at 12 μg mL^{-1} in 1× Tris/borate/EDTA (TBE) buffer, 2.5 V. The compacted DNA layer appears as d) a dark zone when illuminated from above, and e) a brightly reflective zone when illuminated from the side. f) The reflective zone dissipates within 5–10 s after the potential is removed, and g) can be transported between neighboring electrodes upon switching the potential. h–j) Similar reflectivity is observed with proteins. Unlabeled egg white lysozyme (initially at 10 mg mL^{-1} in 1× TBE, 2.5 V) becomes visible within 10–20 s either h) at the cathode, pH 8, or i) at the anode, pH 11. j) Unlabeled prostate specific antigen (initially at 0.1 mg mL^{-1} in phosphate-buffered saline (PBS) at pH 7.2, 2.5 V). k) Label-free detection of heptakis(6-*O*-sulfo)-β-cyclodextran (MW = 1849 Da) initially at 100 μg mL^{-1} in 1× TBE, 3 V. Scale: all electrodes are 50 μm wide horizontally.

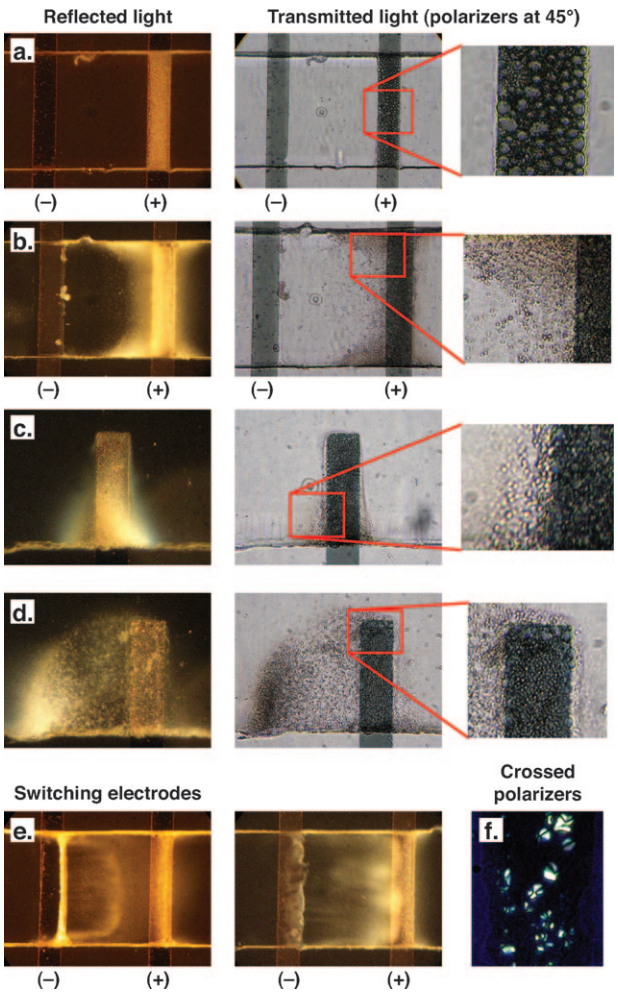

Figure 2. a–d) Reflective zones evident when unlabeled DNA is compacted and viewed under oblique white light (left) are attributable to formation of a stable microbubble layer that can be seen under transmitted polarized illumination (right). In panel (d) the DNA has become ultra-concentrated by sequentially sweeping across 10 electrodes. e) Microbubbles follow the stabilizing DNA as it migrates from one electrode to the next upon switching the potential (left) and re-accumulate on the new anode (right). f) Birefringent zones sometimes become evident when viewed through crossed polarizers. All experiments were performed using a 100 bp dsDNA ladder initially at 20 μg mL^{-1} in 50 mM histidine with 10% v/v β-mercaptoethanol, 1.8 V applied for 2.5 min. Scale: all electrodes are 50 μm wide horizontally.

zones (Figure 2a). These clouds emerge because the compacted macromolecular film imposes a barrier against transport of electrochemically generated gases produced by hydrolysis, introducing a highly reflective topology that makes label-free detection possible. The microbubble clouds are spatially distributed such that their density is greatest near the microchannel sidewalls (Figure 2b) or corners of electrodes that do not span the entire microchannel width (Figure 2c,d) suggesting higher levels of DNA enrichment at these locations, likely owing to the steeper electric field gradients present there (Figure S1 in Supporting Information). Upon switching the potential to an adjacent electrode pair, the reflective zone remains largely intact as it migrates toward the new anode indicating that the microbubbles remain stably embedded within the enriched DNA zone (Figure 2e). Birefringent textures are also sometimes evident when viewed through crossed polarizers (Figure 2f), suggesting local attainment of concentrations high enough to trigger transition to an ordered mesophase.[9]

Collection and enrichment of charged macromolecules within these electrode arrays is electrophoretically dominated owing to their internal arrangement within an enclosed microchannel, rendering electroosmotic velocity proportional to the applied potential rather than the electric field[10] (characteristic electrophoretic velocities are about 100 times greater than those due to electroosmosis;[8] Figure S2 in Supporting Information)—a feature that distinguishes this phenomenon from anomalous DNA condensation effects previously reported under AC fields.[11] Consequently, the governing mechanism can be viewed in terms of a local

competition between 1) electrophoretic transport and compaction of charged macromolecules from the bulk solution into a thin film at the electrode surface, and 2) the gas-producing electrochemical reactions responsible for bubble formation (i.e., hydrolysis of water yielding oxygen at the anode and hydrogen at the cathode). Using DNA as a probe to explore these interactions, we observe that the compacted film is only visible with the aid of fluorescent labeling at potentials below the threshold for electrolysis (ca. 1.3 V) (Figure 3a). Microbubble clouds appear as the potential begins to exceed this threshold, accompanied by emergence of strong surface reflectivity (Figure 3b). As the potential is increased further, locally oversaturated gases begin to coalesce into larger bubbles at the cathode after several minutes, but not at the anode where the compacted DNA film is localized (Figure 3c). This behavior is much different than would be expected if the stabilizing film were not present because oxygen bubbles produced at the anode generally exhibit weak adhesion to metal electrodes and should therefore coalesce to a larger size than the cathodically generated hydrogen.[12] If the potential is applied for a sufficiently long time, the stabilizing capacity of the macromolecular film saturates yielding coalescence at the anode, albeit to a lesser extent than at the cathode (Figure 3d and Movies 1 and 2 in the Supporting Information). This coalescence ruptures the compacted film, an effect that becomes visible as a dark zone centered on the anode flanked by bright regions on either side when the DNA is fluorescently labeled (Figure 3e). No surface reflectivity is evident when carboxylated polystyrene beads are substituted for DNA, indicating that the rigid microspheres are unable to adopt a sufficiently dense packing to stabilize a microbubble layer despite their enrichment at the anode (Movies 3 and 4 in the Supporting Information). This mechanism can be further tuned by altering the interplay

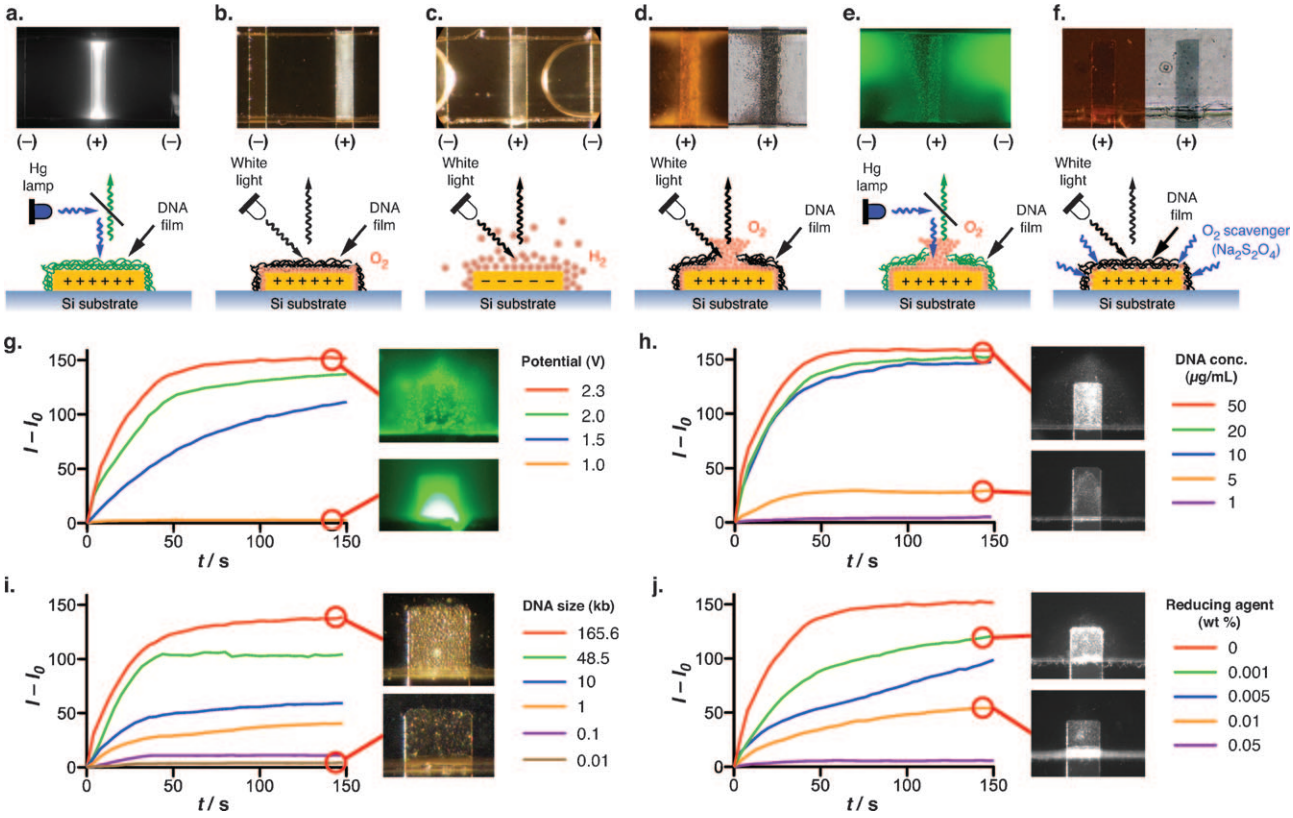

Figure 3. a) Microbubble clouds are not evident below the electrolysis threshold, even though electrophoretically compacted DNA is visible when fluorescently labeled (100 bp dsDNA ladder labeled with YOYO-1 initially at 10 μg mL^{-1} in 50 mM histidine, 0.7 V). b) Above this threshold the electrophoretically compacted DNA film acts to stabilize electrolytically produced oxygen microbubbles, generating strong reflectivity under oblique white light illumination (100 bp dsDNA ladder initially at 12 μg mL^{-1} in 10× TBE, 2.5 V). c) The stabilizing macromolecular film resists local oversaturation so that coalescence into larger bubbles occurs more readily at the cathode (heptakis(6-*O*-sulfo)-β-cyclodextran initially at 100 μg mL^{-1} in 10× TBE, 3 V). d) Oversaturation eventually sets in at the anode under high potentials and/or at long times, rupturing the compacted film (100 bp dsDNA ladder initially at 20 μg mL^{-1} in 50 mM histidine, 1.8 V; images under reflected and transmitted light are shown at the left and right, respectively). e) When fluorescently labeled, the ruptured DNA film is evident by a dark region on the anode flanked by bright zones on either side (100 bp dsDNA ladder labeled with YOYO-1 initially at 10 μg mL^{-1} in the supplied buffer, 1.5 V). f) Microbubble clouds are no longer evident under either reflected (left) or transmitted (right) illumination upon addition of a reducing agent (100 bp dsDNA ladder initially at 20 μg mL^{-1} in 50 mM histidine with 0.06% w/v $Na_2S_2O_4$, 2.5 V applied for 30 min). g–j) Kinetics of microbubble cloud formation. g) Effect of applied potential (unlabeled 100 bp dsDNA ladder initially at 20 μg mL^{-1} in 50 mM histidine). h) Effect of initial concentration (unlabeled 100 bp dsDNA ladder in 50 mM histidine, 2.3 V). i) Effect of DNA length (all samples initially at 20 μg mL^{-1} in 50 mM histidine, 2.3 V). j) Effect of reducing agent $Na_2S_2O_4$ (unlabeled 100 bp dsDNA ladder initially at 20 μg mL^{-1} in 50 mM histidine, 2.3 V). Scale: all electrodes are 50 μm wide horizontally.

between electrochemical and electrophoretic effects as demonstrated by addition of sodium dithionite ($Na_2S_2O_4$), a reducing agent that inhibits microbubble formation by establishing a competitive complexation interaction accelerating uptake of evolved oxygen (Figure 3 f).

We quantified the kinetics of microbubble cloud formation by recording the increase in reflected light intensity as a function of time within a region of interest centered on the active electrode so that representative time constants could be extracted (see Supporting Information). Reflectivity increases at a rate proportional to the applied potential,[13] reaching a plateau within ca. 60 s (Figure 3 g); and kinetics remain unchanged as the initial DNA concentration is varied from 10 to 50 $\mu g\,mL^{-1}$ (Figure 3 h). Changes in DNA length influence the reflected intensity but do not strongly affect the kinetics, with T4 DNA (165 kb) able to stabilize larger microbubbles and generate stronger reflectivity than the much shorter 10 bp fragments (Figure 3 i). The corresponding time constants indicate that the kinetics maintain a similar order of magnitude across the entire ensemble of experimental conditions we investigated, implying that microbubble cloud formation is governed by a fundamentally consistent electrochemical mechanism (Figure S3 and Table S1 in the Supporting Information). Addition of $Na_2S_2O_4$ disrupts this balance, inhibiting development of the microbubble clouds and delaying attainment of an intensity plateau (Figure 3 j). But the magnitude and kinetics of surface reflectivity are eventually restored as the reducing agent is consumed by repeatedly actuating the electrodes (Figure S4 in the Supporting Information).

Applying this phenomenon in the presence of an ionic surfactant instead of DNA makes it possible to produce discrete stabilized microbubbles. We demonstrated this using the anionic surfactant sodium dodecyl sulfate (SDS). At bulk conditions below the critical micelle concentration (CMC; a value of 8.3 mM was assumed),[14] surfactant molecules become compacted at the anode in the same way as DNA but do not attain a sufficiently dense packing to produce strong surface reflectivity (Figure 4 a). Under conditions in the vicinity of the CMC, the electrode surface is initially decorated by a field of reflective spots sparsely arrayed against a dark background, transforming into a dense halo at later times and/or higher potentials (Figure 4 b). At still higher surfactant concentrations (ca. 10× CMC), a more dramatic change occurs whereby discrete encapsulated microbubbles are continuously produced and released into the bulk environment (Figure 4 c). This behavior can be explained by noting that above the CMC micelles from the bulk solution experience compaction at the electrode surface, as opposed to the individual surfactant molecules that predominate at lower concentrations (Figure 4 d). The relatively large size of these micellar structures imposes a steric barrier against adoption of the densely packed arrangement necessary to generate high reflectivity (similar to polystyrene beads; Movies 3 and 4 in the Supporting Information). But because they are immobilized at the electrode surface, the compacted micelles become infused with the electrochemically evolved gas, thereby providing a driving force for production of encapsulated microbubbles. The size and quantity of the microbubbles can be manipulated by adjusting the amplitude and duration of the applied potential, suggesting a versatile manufacturing approach scalable toward both high-volume and small-batch synthesis.

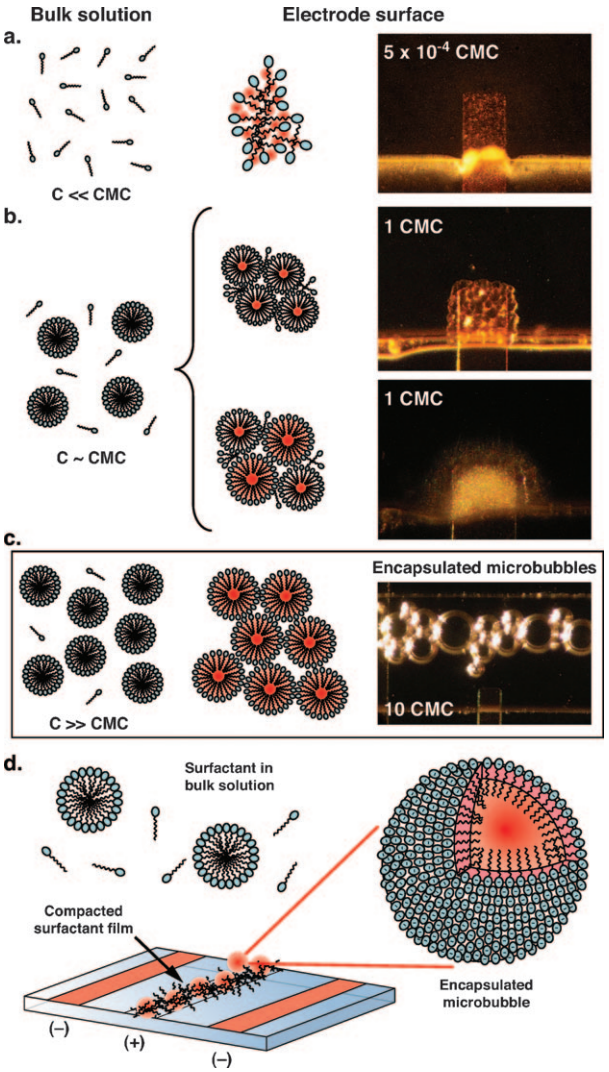

Figure 4. a) Only weak surface reflectivity is evident at the anode when the surfactant concentration is below the CMC (2.8 V applied for 90 s). b) Bright spots appear in the vicinity of the CMC, transforming into a dense opaque halo at higher potentials and/or longer times (top: 3 V applied for 90 s; bottom: 3.5 V applied for 60 s). c) Discrete encapsulated microbubbles are produced at bulk concentrations above the CMC (3 V applied for 60 s for bubble formation, then switched to 5.5 V for 50 ms to trigger release). d) Under these conditions, compacted micelles confined at the electrode surface become infused with electrochemically generated gases. All surfactant solutions contain SDS in 50 mM histidine. Scale: all electrodes are 50 μm wide horizontally.

Received: November 23, 2010
Published online: March 25, 2011

Keywords: analytical methods · DNA detection · electrochemistry · electrophoresis · microbubbles

[1] a) P. S. Epstein, M. S. Plesset, *J. Chem. Phys.* **1950**, *18*, 1505 – 1509; b) S. Ljunggren, J. C. Eriksson, *Colloids Surf. A* **1997**, *130*, 151 – 155; c) L. E. Scriven, *Chem. Eng. Sci.* **1959**, *10*, 1 – 13; d) P. B. Duncan, D. Needham, *Langmuir* **2004**, *20*, 2567 – 2578.

[2] a) M. Borden, *Soft Matter* **2009**, *5*, 716 – 720; b) M. A. Borden, C. F. Caskey, E. Little, R. J. Gillies, K. W. Ferrara, *Langmuir* **2007**, *23*, 9401 – 9408; c) M. A. Borden, G. V. Martinez, J. Ricker, N. Tsvetkova, M. Longo, R. J. Gillies, P. A. Dayton, K. W. Ferrara, *Langmuir* **2006**, *22*, 4291 – 4297; d) E. Dressaire, R. Bee, D. C. Bell, A. Lips, H. A. Stone, *Science* **2008**, *320*, 1198 – 1201; e) D. H. Kim, M. J. Costello, P. B. Duncan, D. Needham, *Langmuir* **2003**, *19*, 8455 – 8466.

[3] a) P. Jauregi, J. Varley, *Trends Biotechnol.* **1999**, *17*, 389 – 395; b) F. Sebba, *J. Colloid Interface Sci.* **1971**, *35*, 643 – 646.

[4] a) J. R. Lindner, *Nat. Rev. Drug Discovery* **2004**, *3*, 527 – 532; b) E. G. Schutt, D. H. Klein, R. M. Mattrey, J. G. Riess, *Angew. Chem.* **2003**, *115*, 3336 – 3355; *Angew. Chem. Int. Ed.* **2003**, *42*, 3218 – 3235.

[5] a) K. W. Ferrara, R. Pollard, M. Borden, *Annu. Rev. Biomed. Eng.* **2007**, *9*, 415 – 417; b) S. Huber, T. Helbich, J. Kettenbach, W. Dock, I. Zuna, S. Delorme, *Radiology* **1998**, *208*, 485 – 489; c) I. Lentacker, B. G. De Geest, R. E. Vandenbroucke, L. Peeters, J. Demeester, S. C. De Smedt, N. N. Sanders, *Langmuir* **2006**, *22*, 7273 – 7278.

[6] a) K. Bjerknes, K. Dyrstad, G. Smistad, I. Agerkvist, *Drug Dev. Ind. Pharm.* **2000**, *26*, 847 – 856; b) U. Farook, E. Stride, M. J. Edirisinghe, *J. R. Soc. Interface* **2009**, *6*, 271 – 277; c) M. Kukizaki, M. Goto, *J. Membr. Sci.* **2006**, *281*, 386 – 396; d) E. C. Unger, T. P. McCreery, R. H. Sweitzer, V. E. Caldwell, Y. Wu, *Invest. Radiol.* **1998**, *33*, 886 – 892.

[7] a) A. M. Gañán-Calvo, J. M. Gordillo, *Phys. Rev. Lett.* **2001**, *87*, 274501; b) K. Hettiarachchi, E. Talu, M. L. Longo, P. A. Dayton, A. P. Lee, *Lab Chip* **2007**, *7*, 463 – 468; c) K. Pancholi, E. Stride, M. Edirisinghe, *J. Drug Targeting* **2008**, *16*, 494 – 501; d) J. I. Park, Z. Nie, A. Kumachev, A. I. Abdelrahman, B. P. Binks, H. A. Stone, E. Kumacheva, *Angew. Chem.* **2009**, *121*, 5404 – 5408; *Angew. Chem. Int. Ed.* **2009**, *48*, 5300 – 5304; e) J. H. Xu, S. W. Li, Y. J. Wang, G. S. Luo, *Appl. Phys. Lett.* **2006**, *88*, 133506.

[8] F. A. Shaikh, V. M. Ugaz, *Proc. Natl. Acad. Sci. USA* **2006**, *103*, 4825 – 4830.

[9] a) F. Livolant, A. Leforestier, *Prog. Polym. Sci.* **1996**, *21*, 1115 – 1164; b) M. Nakata, G. Zanchetta, B. D. Chapman, C. D. Jones, J. O. Cross, R. Pindak, T. Bellini, N. A. Clark, *Science* **2007**, *318*, 1276 – 1279; c) Z. Reich, E. J. Wachtel, A. Minsky, *Science* **1994**, *264*, 1460 – 1463; d) R. L. Rill, T. E. Strzelecka, M. W. Davidson, D. H. Van Winkle, *Physica A* **1991**, *176*, 87 – 116.

[10] T. E. McKnight, C. T. Culbertson, S. C. Jacobson, J. M. Ramsey, *Anal. Chem.* **2001**, *73*, 4045 – 4049.

[11] a) S. Magnúsdóttir, H. Isambert, C. Heller, J.-L. Viovy, *Biopolymers* **1999**, *49*, 385 – 401; b) L. Mitnik, C. Heller, J. Prost, J.-L. Viovy, *Science* **1995**, *267*, 219 – 222.

[12] a) L. J. J. Janssen, C. Sillen, E. Barendrecht, S. J. D. Vanstralen, *Electrochim. Acta* **1984**, *29*, 633 – 642; b) D. Kohlheyer, J. C. T. Eijkel, S. Schlautmann, A. van den Berg, R. B. M. Schasfoort, *Anal. Chem.* **2008**, *80*, 4111 – 4118.

[13] a) S. H. Chiu, C. H. Liu, *Lab Chip* **2009**, *9*, 1524 – 1533; b) S. J. Yang, P. C. Tsai, E. S. Kooij, A. Prosperetti, H. J. W. Zandvliet, D. Lohse, *Langmuir* **2009**, *25*, 1466 – 1474.

[14] A. Cifuentes, J. L. Bernal, J. C. Diez-Masa, *Anal. Chem.* **1997**, *69*, 4271 – 4274.

